6-1-2017

EC03089−6421: A new, very rapidly pulsating sdO star

D. Kilkenny

H. L. Worters

R. H. Østensen
Missouri State University

Recommended Citation

Kilkenny, D., H. L. Worters, and R. H. Østensen. "EC03089− 6421: a new, very rapidly pulsating sdO star." Monthly Notices of the Royal Astronomical Society 467, no. 4 (2017): 3963-3969.

Monthly Notices
of the
ROYAL ASTRONOMICAL SOCIETY

MNRAS **467,** 3963–3969 (2017)
Advance Access publication 2017 January 11

doi:10.1093/mnras/stx063

EC03089−6421: a new, very rapidly pulsating sdO star

D. Kilkenny,[1]★ H. L. Worters[2] and R. H. Østensen[3]

[1]*Department of Physics, University of the Western Cape, Private Bag X17, Bellville 7535, South Africa*
[2]*South African Astronomical Observatory, PO Box 9, Observatory, Cape Town 7935, South Africa*
[3]*Department of Physics, Astronomy and Materials Science, Missouri State University, 901 S. National, Springfield, MO 65897, USA*

Accepted 2017 January 9. Received 2017 January 8; in original form 2016 November 30

ABSTRACT

EC 03089−6421, classified sdO in the Edinburgh-Cape (EC) blue object survey, is shown to have unusually rapid pulsations with a dominant frequency near 32 mHz (amplitude ∼0.02 mag; period 31.1 s) – which appears to be strongly variable in amplitude on time-scales of hours and days – and a generally weaker frequency near 29 mHz (amplitude ∼0.004 mag; period 34.2 s), which is also variable in amplitude. This star varies at twice the frequency of any known hot subdwarf pulsator. Although the low-resolution EC spectrogram appears very similar to those of DAO stars, our analysis derives $T_{\rm eff}$ = 40 200 ± 1600 K; log g = 6.25 ± 0.23 and log N(He)/N(H) = −1.63 ± 0.55; more recent spectrograms give $T_{\rm eff}$ = 37 400 ± 1000 K; log g = 5.70 ± 0.13 and log N(He)/N(H) = −2.02 ± 0.17, both of which indicate that the gravity is too low for a white dwarf star, although the low temperature derived from the Balmer lines is at odds with the absence of neutral Helium and the strength of He II 4686. It is possible that EC 03089−6421 is a field analogue of the ω Cen sdO variables.

Key words: stars: individual: (EC 03089−6421) – stars: oscillations.

1 INTRODUCTION

Studies of the later stages of stellar evolution – hot subdwarf and white dwarf stars – have been enormously enhanced over the last few decades by the continuing discovery of new classes of pulsators within these broader groups.

Pulsating white dwarf stars fall into well-defined temperature regions on the white dwarf cooling tracks and include the DAV (or ZZ Ceti stars), DBV (V777 Her) and DOV (GW Vir) variable types, discovered by Landolt (1968), Winget et al. (1982) and McGraw et al. (1979), respectively. More recently, carbon-rich DQ stars have been found to pulsate (Montgomery et al. 2008) and pulsations have been discovered in extremely low-mass white dwarf stars (Hermes et al. 2012, 2013). Additionally, Kurtz et al. (2013) describe a new category of pulsators, the 'hot DA' stars – at around 30 000 K, much hotter than classical DAV stars. White dwarf pulsation periods lie mostly in the range ∼100–1000 s and, with the possible exception of the low-mass white dwarf stars, are well-understood in terms of non-radial gravity mode (g mode) oscillations (see the comprehensive reviews by Fontaine & Brassard 2008; Winget & Kepler 2008).

The first pulsating hot subdwarfs to be discovered were the rapidly pulsating sdB stars (sdBV$_r$; Kilkenny et al. 1997) which have very short periods (typically ∼2 to 3 min) and are p-mode pulsators (Charpinet et al. 1996). They usually have several oscillation frequencies – in some cases over 40 frequencies have been detected. A few years later, the somewhat cooler group of slowly pulsating sdB stars (sdBV$_s$) was discovered by Green et al. (2003) and are multiperiodic g-mode pulsators with periods of the order of an hour. A small number of stars have been found to exhibit both p- and g-mode variations (Oreiro et al. 2004; Schuh et al. 2006) and are usually referred to as hybrid pulsators. In 2005, the only known He-sdB pulsator, LS IV −14°116, was discovered (Ahmad & Jeffery 2005) with periods in the 30–90 min range, and turned out to have extraordinary metal abundances, including strontium, yttrium and zirconium at 10 000 times solar abundance (Naslim et al. 2011). Finally, the first sdO pulsator was discovered (Woudt et al. 2006) with nine periods between 1 and 2 min. At the time of writing, only a second example of a field pulsating sdO star is known (EO Ceti = PB8783; Østensen 2012), although sdO pulsators have been found in ω Cen at rather lower temperatures (∼50 000 K) than the field equivalents (Randall et al. 2011, 2016) and may represent a separate class of subdwarf variable.

As with the white dwarfs, the pulsating sdB stars provide the opportunity to model the structure of stars via identification of pulsation modes (see for example, Van Grootel et al. 2008 and Charpinet et al. 2008), and – potentially – to determine the rate of evolution via secular frequency changes caused by radius/mean density changes. Additionally, Silvotti et al. (2007) detected a giant planet orbiting the sdBV star HS 2201+2610 (V391 Peg) by measuring timing shifts in the pulsations due to stellar motion around the barycentre.

The *Kepler* mission (Borucki et al. 2010), designed to search for exoplanets has substantially contributed to the study of all types

★ E-mail: dkilkenny@uwc.ac.za

of variable star – the superlative data quality, the ∼3 yr almost uninterrupted baseline and the high cadences of observation providing many new insights. As examples in the hot subdwarf field, new discoveries include the detection of unexpectedly long rotation periods – even in close binaries (Pablo et al. 2012); the clear demonstration of stochasticity in the pulsations of an sdB star (Østensen et al. 2014); the discovery of orbital Doppler beaming in sdB + WD binaries (Bloemen et al. 2011; Telting et al. 2012); radial differential rotation in a hybrid pulsator (Foster et al. 2015) and even the inference of orbiting Earth-like planets (Charpinet et al. 2011).

A space mission currently being planned – the Transiting Exoplanet Survey Satellite (TESS; Ricker et al. 2014) will search for planets around the brightest (and therefore generally nearby) stars. Like *Kepler*, TESS will have guest investigator opportunities; unlike *Kepler*, it will cover essentially the whole sky, with continuous coverage for about a year in large regions around the ecliptic poles. The intersection of preparations for the TESS mission with our work on Edinburgh–Cape (EC) survey stars has led to the discovery reported here.

2 EC 03089−6421

EC 03089−6421 was detected in zone 3 of the EC survey (Kilkenny et al. 2015) which lists a spectral type of sdO and photometry $V = 14.80$, $(B - V) = -0.35$ and $(U - B) = -1.25$. Coordinates from the survey are: $\alpha = 3^{\rm h}08^{\rm m}58\overset{\rm s}{.}7$; $\delta = -64^\circ21'53''$ (1950.0). The star had been picked up much earlier in the BPS survey (BPS CS 31064−0017; Beers, Preston & Schectman 1992 with photometry $V = 14.75$, $(B - V) = -0.34$ and $(U - B) = -1.18$ by Norris, Ryan & Beers 1999) but, to our knowledge, no other spectral type exists. Upon re-examination of the EC spectrogram, we realized that it strongly resembles that of a DAO star. Fig. 3 in the white dwarf spectral atlas of Wesemael et al. (1993) shows spectra of several of these stars and EC 03089−6421 is very similar to S 216, classified DAO1 in the atlas. Wesemael et al. (1993) describe DAO stars as having broad, shallow H lines; weak, sharper He II 4686 and no other ionized Helium lines. In the examples they show, most do not have He I. (Compare with our Fig. 1.) These stars are rare and are not known to pulsate – although the theoretical possibility was predicted nearly 20 yr ago (Charpinet et al. 1997). We return to the spectroscopy of EC 03089−6421 in Section 5.

Because of the rarity of pulsating sdO stars, EC 03089−6421 was included in our programme to get continuous photometry of interesting EC stars and we obtained a short run in 2016 January. The light curve was not noticeably variable and we had not derived a periodogram until a request was received from TESS guest investigators for any indication of variability in a sample of stars near the South Ecliptic pole. The peridogram of EC 03089−6421 showed evidence for peaks significantly above noise at about 68.4 and 93.7 s, which prompted the current work (and turned out to be aliases of the true pulsation frequencies).

3 PHOTOMETRY

The photometry described in this paper was obtained at the Sutherland site of the South African Astronomical Observatory (SAAO) using the 1m telescope with the STE3 CCD photometer and a new 1 m telescope (currently being commissioned) with the Sutherland High-Speed Optical Camera (SHOC).

The STE3 CCD is a 512 × 512 detector which has a read-out time of a little over 6 s when pre-binned 2 × 2, the mode used for all our observations. No filter was used in order to maximize counts.

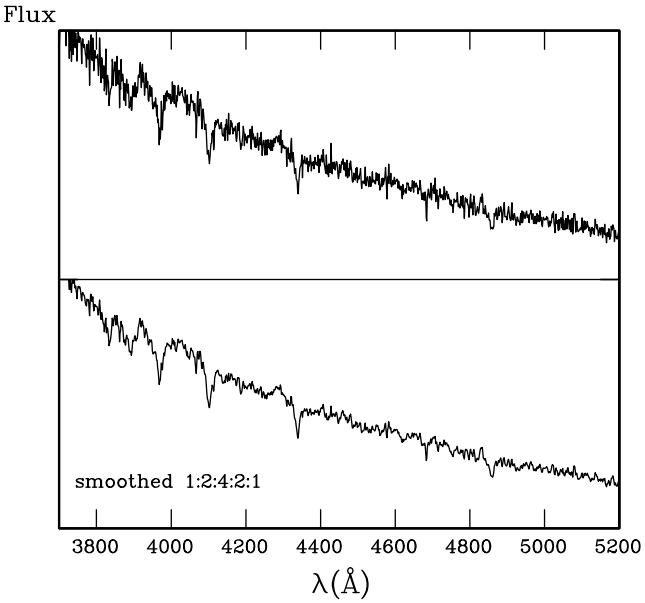

Figure 1. Edinburgh–Cape spectrogram for EC 03089−6421. The upper figure is the wavelength- and flux-calibrated spectrogram; the lower figure is the same data smoothed with a five-point running mean in the ratio 1:2:4:2:1. He II 4686 is present; other lines are of the Balmer series of hydrogen. In the unsmoothed spectrogram, the signal/noise (S/N) varies from ∼12 near 4900 Å to ∼25 near 4000 Å.

Reduction of the CCD frames and magnitude extraction were performed using software based on the DOPHOT program described by Schechter, Mateo & Saha (1993). The STE3 CCD has a small field of view (about 2 × 2 arcmin^2 on the 1 m telescope) so that only one, slightly fainter, star was available for differentially correcting the photometry. We have therefore avoided correcting the data (unless cloud affected the observations) and have removed the effect of atmospheric extinction using a quadratic.

The SHOC instrument uses an Andor E2V CCD and works in frame-transfer mode (with 1024 × 1024 active pixels) so that the read-out time is effectively zero. It has been designed to run at up to 20 frames s^{-1} with high-accuracy timing for each frame. Full details of the system can be found in Coppejans et al. (2013). The SHOC data were reduced using an in-house SAAO aperture photometry pipeline based on IRAF routines and again, no filter was used. On the new 1 m telescope, the camera has a field of view of 5.7 × 5.7 arcmin^2 so that several relatively bright stars were available for differential correction of the photometry.

Because both CCDs were used without optical filters and have similar response curves, and because there is no direct overlap between data from the two systems, it is not possible to make any amplitude/colour comparisons with the current observations.

Table 1 is a log of the photometry used in this paper. Note that in the table, the baseline of observation, $t_{\rm run}$, is often significantly longer than the cycle time ($t_{\rm cyc}$) multiplied by the number of frames. This is because it was sometimes necessary, for various operational reasons, to stop and restart runs (especially with the new telescope still being commissioned) and because on most nights, some frames were rejected due to poor atmospheric conditions. The night of November 6/7 is listed as two separate runs because there was a gap of nearly 3 h between them (rather than just a minute or two).

Table 1. Observing log for EC 03089−6421. t_{run} is the total baseline of the observing run; t_{exp} is the frame exposure time; t_{cyc} is the cycle time – the time between exposures including CCD read-out.

Date 2016 Oct/Nov	Camera	t_{run} (s)	t_{exp} (s)	t_{cyc} (s)	Frames
26/27	STE3	3430	10	16	210
	STE3	5705	5	11	500
	STE3	2362	2	8	282
	SHOC	2406	2	2	1198
	SHOC	1496	1	1	1432
27/28	STE3	3615	5	11	318
	STE3	3842	5	11	336
28/29	STE3	6484	4	10	617
29/30	STE3	11 395	5	11	995
30/31	STE3	11 372	5	11	998
31/01	STE3	10 574	5	11	927
01/02	STE3	10 232	5	11	878
	SHOC	9858	1	1	8897
	SHOC	5703	0.56	0.56	8668
03/04	SHOC	3661	1	1	3308
05/06	SHOC	2696	1	1	2479
	SHOC	3295	3	3	1037
06/07	SHOC	2133	1	1	1944
	SHOC	6402	1	1	5146
15/16	SHOC	1811	1	1	1804

4 FREQUENCY ANALYSIS

The frequency analysis described in this section was carried out with Darragh O'Donoghue's EAGLE program which uses the Fourier transform method of Deeming (1975) as modified by Kurtz (1985).

Because we were initially expecting variations in the range 60–90s, we started with cycle times of ∼16 s using the STE3 camera (as listed in Table 1). When we realized we were dealing with significantly shorter periods, we reduced the exposure times to 5 s (cycle time ∼11 s) and also managed to break into the commissioning of the new 1m telescope to use the SHOC camera with much shorter cycle times – the increased temporal resolution, of course, carries a significant reduction in signal/noise (S/N) for the individual observations. Fig. 2 shows a small section of the SHOC photometry from October 26/27 with a cycle time of 2 s. A variation around 30 s is clearly present and there is no obvious multiperiodic beating. Fig. 3 shows the amplitude spectra from all the SHOC data on the 26/27 – the principal peak has a period of 31.1 s (32.1 mHz) and an amplitude of 0.016 mag. A second peak – at only ∼3 times the noise – has a period of 34.2 s (29.3 mHz) and an amplitude of 0.003 mag.

4.1 STE3 data

To illustrate the STE3 results, we show in Fig. 4 the amplitude spectrum from the night of October 30/31 – one of the best nights we had, with seeing around an arcsecond or better for the whole night. The 31.1 and 34.2 s periods are abundantly clear and it appears that there is still signal around 31 s after removal of the main frequency.

Fig. 5 shows the periodograms on a compact scale for each night of STE3 data and Table 2 lists the extracted frequencies. It is immediately clear that the amplitude of the principal variation at 31.1 s declines steadily throughout the week, though the 34.2 s variation remains fairly constant. Interestingly, the amplitude of pulsation appears to show a very obvious increase during the night of

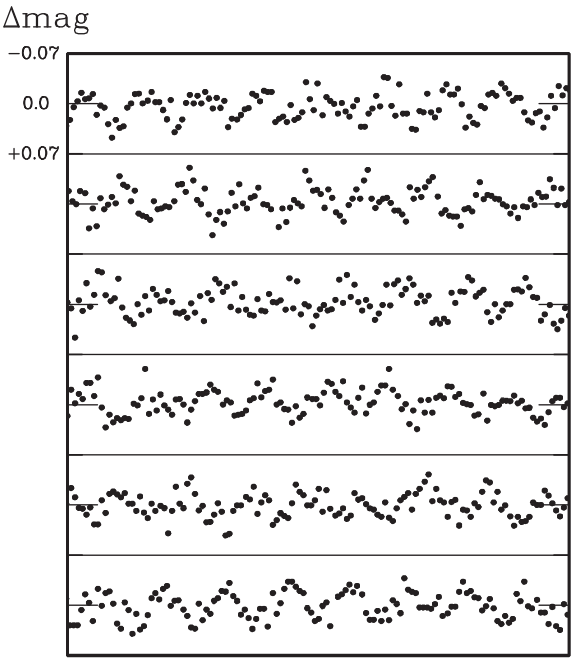

Figure 2. A sample of the 2016 October 26/27 SHOC observations of EC 03089−6421 with the mean magnitude removed. The data points are every 2 s and run left-to-right and top-to-bottom. The length of each panel is 0.003 d – about 260 s.

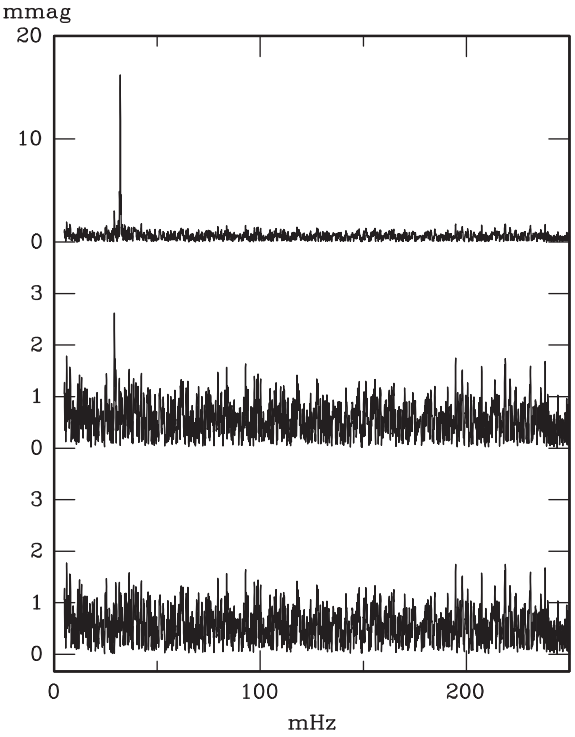

Figure 3. The top panel is the amplitude spectrum for all the SHOC observations from 2016 Oct 26/27. The middle panel shows the same after the removal of the very strong frequency at 32.12 mHz (31.13 s); the bottom panel after the additional removal of the next strongest frequency at 29.27 mHz (34.17 s). Note the different ordinate scale for the upper panel.

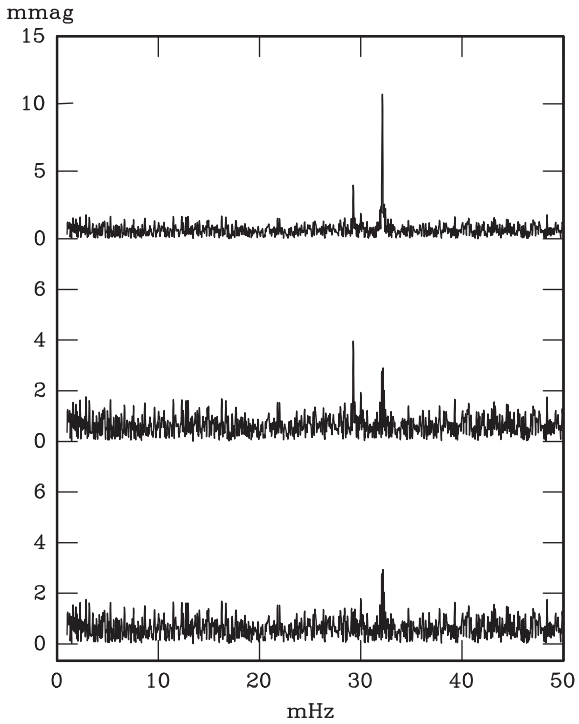

Figure 4. The top panel is the amplitude spectrum for the STE3 observations from 2016 October 29/30. The middle panel shows the same after the removal of the very strong frequency at 32.12 mHz (31.13 s); the bottom panel after the additional removal of the next strongest frequency at 34.20 s (29.2 mHz); see text for discussion. Note the different ordinate scale for the upper panel.

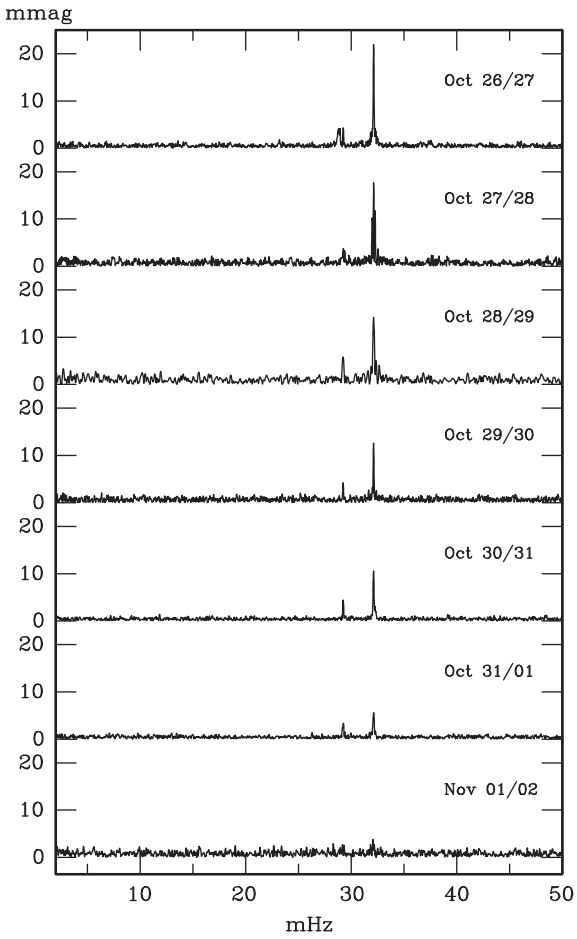

Figure 5. Amplitude spectra for each night of the STE3 observations.

October 26/27 and a decline during the night of October 30/31 – Fig. 6 shows a plot of the latter, condensed in time. The night was of good quality and the star was only observed between air masses of about 1.30 and 1.18, rising, culminating and starting to set. The other star of comparable brightness in the field does not show this effect and it is not so visually obvious for EC 03089−6421 on the other nights. However, if we search for other periods near 31 s, we find on five nights a period near 31.19 s and on three nights a period near 31.09 s with amplitudes ∼0.002–0.003 mag (rather close to noise, but convincing by virtue of appearing on several nights). The frequency differences are equivalent to amplitude modulation on a time-scale ∼6–8 h, which is consistent with what we see in Fig. 6. Thus, the apparent amplitude change seems to persist on several

Table 2. Frequencies extracted on a night-by-night basis. The final column is the root-mean-square error in each periodogram, measured around (but not including) the 29–32 mHz region.

2016 Oct/Nov	Frequency (mHz)	Amplitude (mag)	*P* (s)	Frequency (mHz)	Amplitude (mag)	*P* (s)	rms (mag)
SHOC							
26/27	32.12	0.016	31.13	29.25	0.002	34.18	0.0009
STE3							
26/27	32.13	0.022	31.12	29.25	0.004	34.19	0.0006
27/28	32.13	0.018	31.13	29.25	0.004	34.19	0.0009
28/29	32.13	0.014	31.13	29.22	0.006	34.22	0.0011
29/30	32.12	0.013	31.13	29.24	0.004	34.20	0.0009
30/31	32.12	0.011	31.13	29.24	0.004	34.20	0.0005
31/01	32.13	0.006	31.12	29.26	0.003	34.17	0.0005
01/02	32.06	0.004	31.19	29.18	0.003	34.27	0.0010
SHOC							
01/02	32.07	0.005	31.18	29.28	0.002	34.16	0.0004
03/04	32.12	0.012	31.13	29.26	0.010	34.18	0.0006
05/06	32.13	0.014	31.12	29.25	0.015	34.19	0.0011
06/07	32.17	0.004	31.08	29.26	0.005	34.18	0.0007
15/16	32.17	0.021	31.09	–	<0.005	–	0.003

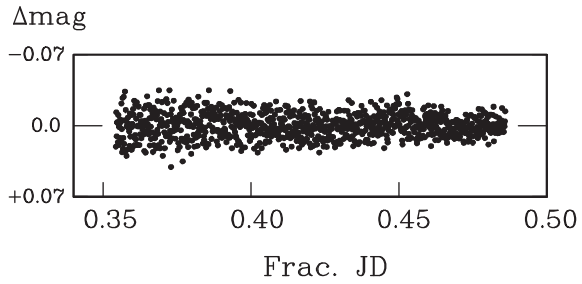

Figure 6. Condensed observations from 2016 October 30/31.

nights – in addition to the overall decline seen during the course of a week.

Next, we analysed all the STE3 data together, calculating the amplitude spectrum, removing the highest peak (pre-whitening), calculating the next highest peak, removing both peaks with a simultaneous least-squares solution and so on. Initially, we found weak evidence for low-frequency peaks – periods ∼1200–1400 s – but when the data were split into two parts and analysed separately, these peaks were not consistent from part to part and so we consider them to be spurious. We also find that – as with individual nights – we can extract frequencies very close to the 31.1 and 34.2 s variations. In the case of the former, we find frequencies separated by about 1 μHz and ∼35 μHz (amplitudes ∼0.005 mag) from the main frequency which, if due to the software attempting to reproduce complex amplitude changes with multiple close frequencies, would result in time-scales of ∼11 and 0.3 d, respectively, roughly what we observe.

4.2 SHOC data

Because the STE3 data showed such a marked decline in amplitude during the observing week, we continued to try for commissioning time on the new 1 m telescope + SHOC. We also wanted to obtain data with as high a time resolution as possible – in full-frame readout with pre-binning appropriate to the typical seeing conditions, this is about 0.56 s. The SHOC runs in early November are listed in Table 1 and the highest extracted peaks in Table 2. As can be seen from Table 2 and Fig. 7, the pulsation amplitudes increase and then decrease during the second week of observations, but the 34.2 s variation becomes the strongest, despite appearing to be relatively stable during the previous week.

A short, isolated run on November 15/16 shows the 31.1 s variation at 0.021 mag – about as strong as we have observed it to be – with the 34.2 s variation not detected at the 0.005 mag level (the short run means the noise level is quite high).

As with the STE3 data, we have analysed all the early November SHOC data combined. We find that the peaks near 31.1 and 34.2 s are actually small clusters of peaks; the three largest amplitudes for each group are listed in Table 3. Again, it seems most likely that these are created by the software fitting several very close frequencies to reproduce fairly rapid amplitude variations or by the sort of phase variations observed in KIC 2991276 by Østensen et al. (2014). From the examples listed in Table 3, the frequency differences are from a few to a few tens of μHz, corresponding to periods from about a quarter of a day to three days.

We find no coherent low-frequency variations. Between 0 and 0.01 Hz (100 s) there are no peaks as large as 0.005 mag – essentially noise. Additionally, there are no obvious very high frequencies. We calculated periodograms for the 2016 November 1/2 observations – the longest run of SHOC data, which is comprised only of

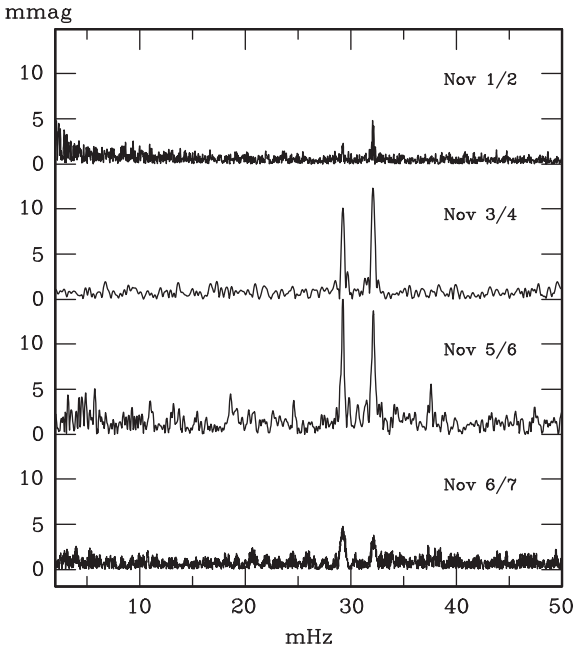

Figure 7. Amplitude spectra for each night of the early November SHOC observations.

Table 3. Six highest frequencies extracted from the combined SHOC data for 2016 November 1–6.

Frequency (mHz)	Amplitude (mag)	*P* (s)	Frequency (mHz)	Amplitude (mag)	*P* (s)
32.081	0.007	31.17	29.263	0.005	34.17
32.129	0.005	31.12	29.226	0.004	34.22
32.134	0.003	31.14	29.290	0.003	34.14

observations of 1 or 0.56 s cadence, and there are no peaks higher than about 0.001 mag – again, essentially noise – between 0.05 and 1 Hz (20–1 s).

5 ATMOSPHERIC PARAMETERS

In Section 2, we noted that although EC 03089−6421 was classified sdO in the EC survey, the spectrum is remarkably similar to that of DAO stars in that we detect He II 4686 but no other ionized Helium lines (unlike the sdO stars) and there is no He I. The single low-dispersion EC spectrogram was obtained on 1993 August 18 with the Unit Spectrograph (at that time, equipped with a Reticon detector) on the SAAO 1.9 m telescope using grating 6 which has a coverage about 3600–5400 Å and resolution ∼3.5 Å. The spectrogram was reduced with in-house SAAO software and fitted to the pure H+He NLTE grid of Stroeer et al. (2007) with the fitting procedure used by Napiwotzki (1999). The fit converges to a solution of $T_{\rm eff} = 40200 \pm 1600$ K; $\log g = 6.25 \pm 0.23$ and $\log {\rm N(He)/N(H)} = -1.63 \pm 0.55$, so that our derived surface gravity appears to be too low for the star to be a white dwarf, which have $\log g > 7$ – with the great majority having $\log g > 7.5$ (Fontaine & Brassard 2008, Nelemans 2010, for example).

Subsequent to the discovery of variability in EC 03089−6421, we were also able to obtain grating 4 spectrograms with the refurbished Cassegrain spectrograph (with an E2V 2048 × 512 CCD detector) on the SAAO 1.9 m telescope. These were reduced using standard IRAF tasks. Grating 4 has twice the dispersion of

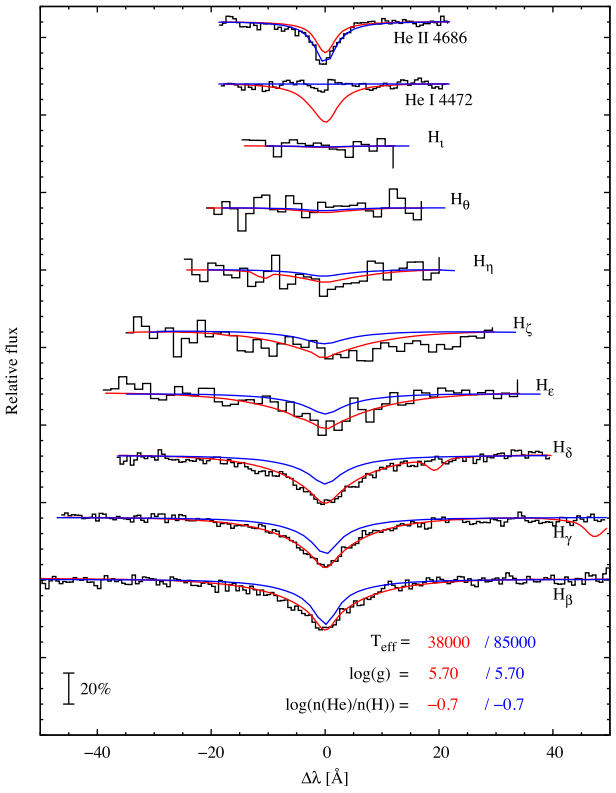

Figure 8. Atmospheric parameters derived from the EC survey and new spectrograms. Note that the cooler model fits the Hydrogen lines well and the Helium lines very poorly; the hotter model, the other way around.

grating 6 – but, of course, half the wavelength range; only Hβ, He II 4686, H γ and H δ were covered. We averaged three spectrograms (giving an S/N $\sim$ 50) and the fit to these is $T_{\rm eff} = 37\,400 \pm 1000$ K; log $g = 5.70 \pm 0.13$ and log N(He)/N(H) $= -2.02 \pm 0.17$, but note that the fit is less sensitive to surface gravity due to the absence of higher order Balmer lines. The errors quoted are the formal fitting errors when matching the individual spectra to the model grids, and do not reflect any systematic errors inherent in the models, in particular, the complete neglect of any elements besides H and He. The convergence of both fits are dominated by the Balmer lines, and clearly show that the models are incapable of simultaneously fitting the Balmer and Helium lines. If we use only the He lines, the fit converges to a temperature as high as 85 000 K, and a higher He abundance, log (N(He)/N(H) $= -0.7$. The fit was computed keeping log g fixed to 5.7, as there is not sufficient information in the He II line to provide a useful constraint on log g. Fig. 8 shows the relevant regions of the spectra (using the lines from the new spectrum where available), and overplotting the model spectrum for 38 000 and 85 000 K in red and blue, respectively. This problem is similar to that observed in EC 11481−2303, described by Rauch, Werner & Kruk (2010) and known as the Balmer-line problem (Werner 1996; Bergeron et al. 1993), in which neglecting sufficient metal opacities in model-atmosphere calculations produces incorrect temperature stratification in the line-forming regions. The problem can be resolved by strongly increasing the abundance of iron-group elements. In light of this, it is reasonable to assume that the temperature of the star is much higher than indicated by our Balmer-line fits, but better spectroscopy and advanced models would be required to get useful constraints, especially on the surface gravity.

6 DISCUSSION

It seems very unlikely that the variations observed in EC 03089−6421 could be due to stellar rotation; the fact that we detect two frequencies in itself makes this improbable. If we assume the stellar radius is 0.1 $R_\odot$, then a spin period of 31 s, would give the star an equatorial velocity of $\sim$14 000 km s^{-1}. Alternatively, if we make the simplistic argument that a star will break up when the centrifugal force produced by rotation is greater than the surface gravity, with $M = 0.5\,M_\odot$ and $R = 0.1\,R_\odot$, the limiting spin period is about 450 s. Even for a white dwarf with $R = 0.01\,R_\odot$ the limit is $\sim$15 s. And with a log $g \sim 6$, the star is clearly very far from this situation. Analogous arguments can be made for variations from a binary system – it is difficult to explain two close frequencies and the required orbital velocities would be enormous. The simplest and most probable explanation of the observed variations is that we are seeing pulsations. Indeed, there exist models (fig. 13 of Randall et al. 2016) with periods similar to those reported here, albeit at temperatures in excess of 64 000 K. Given the uncertainties discussed in Section 5, this is not implausible for EC03089−6421. As far as we are aware, this star is then the fastest known pulsator.

The first recognized sdO pulsator SDSS J160043.6+074802.9 (=V499 Ser) was found by Woudt et al. (2006) with a dozen or more variations in the range 60–120 s. Atmospheric parameters $T = 70\,000 \pm 5000$ K and log $g = 5.25 \pm 0.3$ were derived by Rodríguez-López et al. (2010) and $T = 68500 \pm 1770$ K and log $g = 6.09 \pm 0.07$ by Latour et al. (2011).

PB 8783 (= EO Ceti) was the second pulsating subdwarf to be discovered with six periods in the range 102–135 s (Koen et al. 1997), but was not recognized as an sdO star at the time because of the difficulty in analysing the composite spectrum in a binary system (O'Donoghue et al. 1997). A multisite campaign found 11 variations in the range 94–136 s (O'Donoghue et al. 1998). The discovery paper determined $T = 38\,000 \pm 1000$ K and log $g = 5.8 \pm 0.2$ but, using much more extensive spectroscopy, Østensen (2012) was able to show that the subdwarf was an O-type with $T = 52\,000$ K and log $g = 6.05$.

In this paper, we have shown that EC 03089−6421 is a very rapid pulsator with two frequencies near 32.1 and 29.2 mHz – periods of 31.1 and 34.2 s, much shorter than observed in the other sdOV stars, or in any pulsating subdwarf (see table 1 of Holdsworth et al. 2017). Both frequencies have quite variable amplitudes – between about 0.2 and 2 per cent on a time-scale of a few days and also varying on a time-scale of hours. From the medium-resolution EC spectrogram, we derive $T_{\rm eff} = 40\,200$ and log $g = 6.25$ – and with better resolution and S/N but fewer lines, $T_{\rm eff} = 37400$; log $g = 5.70 \pm$ and log N(He)/N(H) $= -2.02$. The surface gravity is consonant with the two other sdOV stars but our derivations of temperature are very low for the sdO type, and the absence of He I and strength of He II 4686 indicates a problem in the model fitting. Finally, we see no evidence for a companion – unlike the two other known sdO pulsators in the field.

One possibility, given the relatively low temperature of EC 03089−6421 is that it is a field analogue of the sdO variables found in ω Cen (Randall et al. 2011) – they are typically $\sim$50 000 K. Spectroscopy of the cooler stars ($\sim$48 000 K) in the ω Cen sample (see fig. 2 of Randall et al. 2011; and fig. 8 of Randall et al. 2016) shows that He I is not visible, although the models indicate that at least He I 4471 should be present. He II 4686 is strong, as is He II 5412, but the latter is outside the range of our spectrograms. The other He II lines are quite weak and might be lost in the noise in our data but would, in any case, disappear at a somewhat lower

temperature. Allowing for the fact that our derivations do not match the He II 4686 line well, suggesting a higher temperature than the model fit, it is possible that this star is a cooler ω Cen-type variable. Actually, based on the temperature derived by Østensen (2012), EO Ceti would also fall into the ω Cen instability strip (Randall et al. 2016) – between the hot sdBV$_r$ stars and V499 Ser, the very hot sdOV star (which would then be in a lonely class of one).

At ecliptic coordinates $\lambda = 342.2$; $\beta = -72.7$, EC 03089−6421 is close to the planned continuous viewing zone of TESS (Ricker et al. 2014), which will allow it to be continuously monitored for several consecutive 27 d pointing periods. With proposed sampling as short as 20 s, this relatively bright star will be the perfect object to fully resolve the frequency spectrum of an sdOV star and to test the limits of high-cadence persistent photometric space-based monitoring in the super-Nyquist regime (Murphy, Shibahashi & Kurtz 2013).

ACKNOWLEDGEMENTS

We are indebted to Dr Uli Heber for advice and discussion on the analysis of subdwarf spectroscopy and to the referee, Dr John Telting and Dr Chris Koen for a number of useful comments which have improved the original manuscript. This paper uses observations made at the SAAO and, as always, DK is grateful for generous allocations of telescope time by the SAAO and for the continuing support at the telescope provided efficiently and cheerfully by SAAO staff. This paper is based partly upon work supported financially by the National Research Foundation of South Africa and has made use of the SIMBAD data base and the VizieR catalogue access tool, operated at the Centre de Données astronomiques de Strasbourg in Strasbourg, France.

REFERENCES

Ahmad A., Jeffery C. S., 2005, A&A, 437, L51
Beers T. C., Preston G. W., Schectman S. A., 1992, AJ, 103, 1987
Bergeron P., Wesemael F., Lamontagne R., Chayer P., 1993, ApJ, 407, 85
Bloemen S. et al., 2011, MNRAS, 410, 1787
Borucki W. J. et al., 2010, Science, 327, 977
Charpinet S., Fontaine G., Brassard P., Dorman B., 1996, ApJ, 471, L103
Charpinet S., Fontaine G., Brassard P., Dorman B., 1997, ApJ, 489, L149
Charpinet S., Van Grootel V., Fontaine G., Brassard P., Green E. M., Chayer P., Randall S. K., 2008, A&A, 489, 377
Charpinet et al., 2011, Nature, 480, 496
Coppejans R. et al., 2013, PASP, 125, 976
Deeming T. J., 1975, Ap&SS, 36, 137
Fontaine G., Brassard P., 2008, PASP, 120, 1043
Foster H. M., Reed M. D., Telting J. H., Østensen R. H., Baran A. S., 2015, ApJ, 805, 94
Green E. M. et al., 2003, ApJ, 583, L31
Hermes J. J. et al., 2012, ApJ, 750, L21
Hermes J. J. et al., 2013, ApJ, 765, 102
Holdsworth D. L., Østensen R. H., Smalley B., Telting J. H., 2017, MNRAS, in press
Kilkenny D., Koen C., O'Donoghue D., Stobie R. S., 1997, MNRAS, 285, 640
Kilkenny D., O'Donoghue D., Worters H. L., Koen C., Hambly N., MacGillivray H., 2015, MNRAS, 453, 1879
Koen C., Kilkenny D., O'Donoghue D., van Wyk F., Stobie R. S., 1997, MNRAS, 28, 645
Kurtz D. W., 1985, MNRAS, 213, 773.
Kurtz D. W., Shibahashi H., Dhillon V. S., Marsh T. R., Littlefair S. P., Copperwheat C. M., Gänsicke B. T., Parsons S. G., 2013, MNRAS, 432, 1632
Landolt A. U., 1968, ApJ, 153, 151
Latour M., Fontaine G., Brassard P., Green E. M., Chayer P., Randall S. K., 2011, ApJ, 733, 100
McGraw J. T., Starrfield S. G., Angel J. R. P., Carleton N. P., 1979, in Trevor C. W., ed., SAO Special Report 385, The MMT and the Future of Ground-Based Astronomy. Mount Hopkins Observatory, Arizona, p. 125
Montgomery M. H., Williams K. A., Winget D. E., Dufour P., DeGennaro S., Liebert J., 2008, ApJ, 678, L51
Murphy S. J., Shibahashi H., Kurtz D. W., 2013, MNRAS, 430, 2986
Napiwotzki R., 1999, A&A, 350, 101
Naslim N., Jeffery C. S., Behara N. T., Hibbert A., 2011, MNRAS, 412, 363
Nelemans G., 2010, Ap&SS, 329, 25
Norris J. E., Ryan S. G., Beers T. C., 1999, ApJS, 123, 639
O'Donoghue D., Lynas-Gray A. E., Kilkenny D., Stobie R. S., Koen C., 1997, MNRAS, 285, 659
O'Donoghue D. et al., 1998, MNRAS, 296, 296
Oreiro R., Ulla A., Pérez Hernández F., Rodrguez López C., MacDonald J., 2004, A&A, 418, 243
Østensen R. H., 2012, in Kilkenny D., Jeffery C. S., Koen C., eds, ASP Conf. Ser. Vol. 452, 5th Meeting on Hot Subdwarf Stars and Related Objects. Astron. Soc. Pac., San Francisco, p. 233
Østensen R. H., Reed M. D., Baran A. S., Telting J. H., 2014, A&A, 564, L14
Pablo H. et al., 2012, MNRAS, 422, 1343
Randall S. K., Calamida A., Fontaine G., Bono G., Brassard P., 2011, ApJ, 737, L27
Randall S. K. et al., 2016, A&A, 589, A1
Rauch T., Werner K., Kruk J. W., 2010, Ap&SS, 329, 133
Ricker G. R. et al., 2014. J. Astron. Telesc. Instrum. Syst., 1, 014003
Rodríguez-López C. et al., 2010, MNRAS, 401, 23
Schechter P. L., Mateo M., Saha A., 1993, PASP, 105, 1342
Schuh S., Huber J., Dreizler S., Heber U., O'Toole S. J., Green E. M., Fontaine G., 2006, A&A, 445, 31
Silvotti R. et al., 2007, Nature, 449, 189
Stroeer A., Heber U., Lisker T., Napiwotzki R., Dreizler S., Christlieb N., Reimers D., 2007, A&A, 462, 269
Telting J. H. et al., 2012, A&A, 544, A1
Van Grootel V., Charpinet S., Fontaine G., Brassard P., Green E. M., Chayer P., Randall S. K., 2008, A&A, 488, 685
Werner K., 1996, in Jeffery C. S., Heber U., eds, ASP Conf. Ser. Vol. 96, Hydrogen Deficient Stars. Astron. Soc. Pac., San Francisco, p. 265
Wesemael F., Greenstein J. L., Liebert J., Lamontagne R., Fontaine G., Bergeron P., Glaspey J. W., 1993, PASP, 105, 761
Winget D. E., Kepler S. O., 2008, ARA&A, 46, 157
Winget D. E., Robinson E. L., Nather R. D., Fontaine G., 1982, ApJ, 262, L11
Woudt P. A. et al., 2006, MNRAS, 371, 1497

This paper has been typeset from a TEX/LATEX file prepared by the author.